JOURNAL OF MATERIALS SCIENCE 22 (1987) 965–972

Phase transformations of gel-derived magnesia partially stabilized zirconias

T. Y. TSENG, C. C. LIN
National Chiao Tung University, Hsinchu, Taiwan, Republic of China
J. T. LIAW
Industrial Technology Research Institute, Hsinchu, Taiwan, Republic of China

Both chloride-free (amorphous, group A) and chloride-containing (crystalline, group B) ZrO_2–8.1 mol% MgO powders produced by means of gelatinized coprecipitation have been calcined at 450 to 1450° C and characterized by differential thermal analysis/thermal gravimetric analysis, X-ray diffraction, electron microscopy, and infrared spectroscopy. For both groups A and B, the powder density, chloride content, crystallite size, crystallization temperature, and the initial temperature for metastable tetragonal-to-monoclinic ($T_m \rightarrow M$) transformation decrease with increasing concentration of NH_4OH with which samples were prepared. High-temperature tetragonal-to-cubic transformation of group B also revealed the same relationship, but the inverse for group A. An explanation based on the nature of the Zr–O bond and internal strain have been proposed for both transitions. In addition, it is also found that silica can inhibit both transitions and raise the critical crystallite size for $T_m \rightarrow M$ transitions, but water vapour and chloride have the inverse effect on the $T_m \rightarrow M$ transition.

1. Introduction

Although extensive investigations have been made over the last half century, zirconia still remains an interesting subject for ceramic researchers because of its great industrial and scientific uses. The most notable property of zirconia is the phase transition. It has been confirmed that the high-temperature transformation between the tetragonal and monoclinic phases is martensitic [1]; the transition between tetragonal and cubic, on the other hand, has also been suggested as martensitic [2, 3]. For low-temperature transition, most studies have focused on metastable tetragonal to monoclinic phase; only a few works have been done on metastable cubic to monoclinic or tetragonal phase [4–6]. The existence of a metastable phase at room temperature is decided by the method of powder production. Clark and Reynolds [7] have shown that the low-temperature tetragonal form of zirconia is probably identical in structure with the form which is stable between 1000 and 1900° C. Much work has been done in order to explain the source of the metastability of the tetragonal phase [8–12]; nevertheless, unanimous interpretation has not yet been established.

The application of pure zirconia ceramics is restricted due to extensive microcracking caused by the anisotropic volume expansion accompanying tetragonal to monoclinic transition. One solution to this problem is to form solid solutions or "alloys" of cubic zirconia, thus partially stabilized zirconias (PSZ) have found their place and have been extensively investigated. However, most authors focused their studies on thermal and mechanical properties, and research on phase transition of PSZ is rare, especially for the low-temperature transition. The present work aimed at a study of the thermal transformation in MgO–PSZ which is derived from gels. The effects of hydrolytic conditions were observed, and the differences in transition were explained. There are two similar works which have been published by Crucean and Rand [13] and Yoldas [14, 15]. Both groups have shown the significant differences in the ZrO_2 structure as a function of water of hydrolysis or PH value used in the preparation of powders, and thus induce differences in phase transformation, sintering, and crystallization temperature. Nevertheless their attention was still towards the pure ZrO_2, and the MgO–ZrO_2 system remained uninvestigated before the present work.

2. Experimental procedure

2.1. Preparation of samples

The samples were prepared essentially following the method developed by Viechnicki and Stubican [16] but with some modifications for the present work. Table I lists all sample labels and their conditions for preparation. An asterisk denotes chloride-free samples. ZrO_2–8.1 mol% MgO gels were produced by hydrolysing $ZrOCl_2 \cdot 8H_2O$ (Merck 8917, Pro analysi; West Germany) and $Mg(NO_3)_2 \cdot 6H_2O$ (Riedel-deHaën 31415, für analyse, West Germany) in methanol with excess NH_4OH (The Chemical Industry Institute of ITRI, semiconductor grade, ROC). Half of the as-formed gels were washed in turn with 0.2 N NH_4OH and deionized water until chloride could not be detected with 1 M $AgNO_3$ aqueous solution. The chloride-free gels were then dried in vacuum (for 58 h) and ground to amorphous powders. The residual gels were calcined at 450° C in air for 24 h after drying at 100 to 110° C, and then air quenched

0022–2461/87 $03.00 + .12

TABLE I Magnesia partially stabilized zirconia samples

Concentration of NH_4OH	Chloride-containing gel (450° C calcined powder)	Chloride-free gel (powder)
15.35 N	A	A*
8 N	B	B*
2 N	C	C*
0.6 N	D	D*
0.2 N	E	E*
15.35 N + 2 wt % SiO_2	F	F*
15.35 N	G (vacuum dry sample without washing)	

and ground to powders. These calcined powders are crystalline and chloride-containing tetragonal phase.

Additional SiO_2 and NH_4Cl-containing samples have been prepared by the same method except that the SiO_2 was added to a solution of $ZrOCl_2 \cdot 8H_2O$ and $Mg(NO_3)_2 \cdot 6H_2O$ before addition of NH_4OH to produce the SiO_2-containing sample (F and F*), and the gel was dried in vacuum directly, without removing any NH_4Cl to produce the NH_4Cl-containing sample (G). The SiO_2 powder was prepared according to the paper of Sacks and Tseng [17], and the amount of addition were 2% based on the weight of ZrO_2 in Mg–PSZ.

2.2. Calcination

All samples listed in Table I were placed in alumina crucibles and calcined in static air at selected temperatures (450 to 1450° C). Calcination was performed in a tubular quartz furnace (Model MB-71, Mini-Brute Diffusion Furnace, Thermo Products Co., California, USA) for 450 to 1150° C, and a box furnace (Model 840959-1, C and M Inc, New Jersey, USA) for 1250 to 1450° C. Samples were quickly placed in the furnace when the required temperature had been attained, and subsequently air quenched to room temperature after 2 h calcination.

An additional calcination in $H_2O(g)/N_2(g)$ atmosphere at 450, 600 to 1100° C was done to samples A and A* which were put into the furnace when the steam had been generated stably. The steam was produced by a steam generator where water was heated to boiling point and brought into the furnace by nitrogen. The flow rate of nitrogen was 2.94 l min^{-1}, and water was consumed at about 350 ml h^{-1}.

2.3. Characteristic analysis

The chloride content of chloride-containing samples were analysed by the argentometric method [18], and the powder density was determined by using Stereopycnometer (Quantachrome, New York, USA). All chloride-free samples were analysed by differential thermal analysis (DTA) (Model 5000, Ulvac, Yokohama, Japan) and thermal gravimetric analysis (TGA) at a heating rate of 10° C min^{-1} in static air. Both DTA and TGA experiments were simultaneously carried out up to 1100° C against α-Al_2O_3 reference, and the heat effect was based on an R-type thermocouple.

X-ray diffraction (XRD) (Model XC-60, Toshiba, Tokyo, Japan) powder patterns for phase identification were obtained using nickle-filtered Cu$K\alpha$ radiation

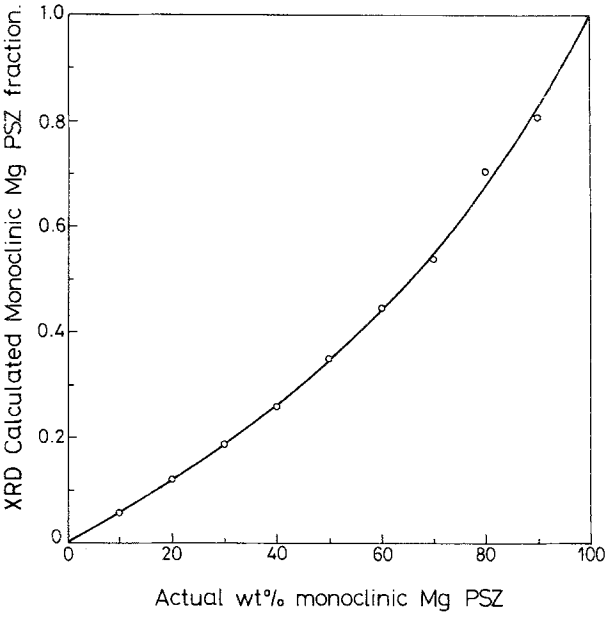

Figure 1 Calibration curve determined from standard mixtures composed of monoclinic and tetragonal phase derived from the calcined Mg–PSZ gels.

with a scanning rate of 1° min^{-1}. An infrared spectrum (Model 260-50, Hitachi Ltd, Tokyo, Japan) was used to assist in phase analysis. Crystallite size was calculated by using the $(1\,1\,\bar{1})_m$ and $(1\,1\,1)_t$ diffraction peaks from the Sherrer relationship [19],

$$D_{hkl} = \frac{0.9\lambda}{\beta_{1/2} \cos \theta} \quad (1)$$

where D_{hkl} is the crystallite size based on the (hkl) reflection, λ the radiation wavelength, β the corrected half-width obtained by using the (1 0 1) peak of low quartz as the standard and the Warren's formula, and θ the Bragg angle. The phase ratios between metastable tetragonal and monoclinic phase, monoclinic and cubic phase in the coexistence region were calculated by considering the intensity of the $(1\,1\,1)_m$, $(1\,1\,\bar{1})_m$, $(1\,1\,1)_t$ and $(1\,1\,1)_c$ reflections using the equations below [20]:

$$f_m = \frac{I_m(1\,1\,1) + I_m(1\,1\,\bar{1})}{I_m(1\,1\,1) + I_m(1\,1\,\bar{1}) + I_t(1\,1\,1)} \quad (2)$$

$$f_c = \frac{I_c(1\,1\,1)}{I_m(1\,1\,1) + I_m(1\,1\,\bar{1}) + I_c(1\,1\,1)} \quad (3)$$

where f_m and f_c are the fractions of monoclinic and cubic phase, respectively, and $I_m(1\,1\,1)$, $I_m(1\,1\,\bar{1})$, $I_t(1\,1\,1)$ and $I_c(1\,1\,1)$ denote the intensity of the $(1\,1\,1)_m$, $(1\,1\,\bar{1})_m$, $(1\,1\,1)_t$, and $(1\,1\,1)_c$ diffraction peaks, respectively. However, Evans *et al.* [21], have shown that errors of up to 20% can be made by using Equation 2 to calculate the amount of monoclinic and tetragonal phase present. To avoid these errors, the calibration curve as shown in Fig. 1 was applied to obtain the actual amount of monoclinic and tetragonal phase present. This calibration curve was obtained from a set of standard mixtures composed of monoclinic and tetragonal phase derived from the calcined Mg–PSZ gels we prepared and the detailed preparation procedure is similar to that given in [21].

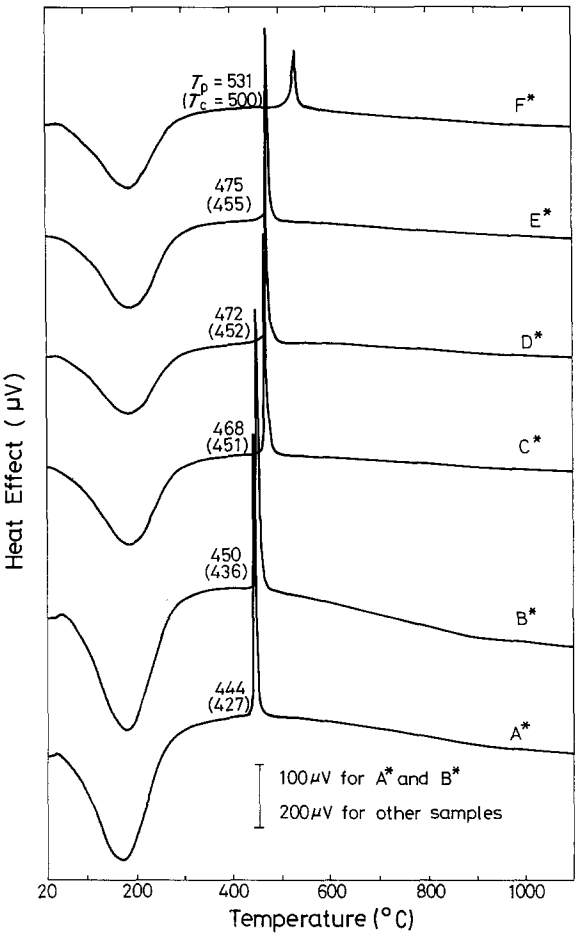

Figure 2 Differential thermal analysis results on chloride-free gels (T_p = temperature of exothermic peak; T_c = crystallization temperature).

In addition, the character of the gels and calcined samples has also been observed using transmission electron microscopy (TEM) (Model H-600, Hitachi Ltd, Tokyo, Japan).

3. Results and discussion

3.1. Characterization of starting materials

Fig. 2 shows the DTA results of chloride-free samples. The numerical values in parentheses denote the crystallization temperatures (T_c). Both T_p and T_c decrease with increasing concentration of NH_4OH except for sample F*. For the present study, the method of gel formation regarded as being an hydrolysis reaction by considering the possible forms of reactants in the solvent, i.e. the reaction may be described as follows (unbalanced):

$$\underset{Mg(NO_3)_2}{ZrOCl_2} + NH_4OH \rightarrow (ZrO_2 \cdot MgO) \cdot xH_2O + NH_4^+ + Cl^- + NO_3^- \xrightarrow{450^\circ C} t\text{-}ZrO_2(MgO) + H_2O(g)$$

where x varied with the conditions and methods employed for drying, and the dried gels before calcination at 450° C were considered hydrous, as pointed out by Blumenthal [22].

The powder density and chloride content of chloride-containing samples descrease with increasing concentration of NH_4OH, as shown in Fig. 3. According to a qualitative analysis, it has been found that there are no free NH_4^+ ions in the soaking solutions of the chloride-containing samples, and the soaking solutions of samples A, B and C are weak basic but neutral or acidic for the others. Combining the results above, it implies that chloride cannot be removed completely at 450° C although the decomposition temperature of NH_4Cl is only 350° C, and chloride ions should be adsorbed chemically onto ZrO_2 (MgO) rather than exist as NH_4Cl. The lower concentration of NH_4OH favours adsorption of chloride ions which rendered the difference in chloride content.

Gels produced under higher NH_4OH concentrations, on the other hand, have been considered to be an assembly of linear or planar polymerized particles which have a larger pore volume and pore size because of coagulation prior to sedimentation during preparation. A similar phenomenon has been observed on ZrO_2 gels prepared at various pHs [13], and on silica prepared by hydrolysis of alkoxide [15]. The differences in powder density as shown in Fig. 3 are possibly a result of the state of the gel. In addition, the chloride content and powder density of the SiO_2-containing sample (sample F) as shown in Fig. 3 are higher than samples not containing SiO_2 which are produced under the same concentration of NH_4OH (15.35 N). For this case, the higher density is possibly attributable to the small ionic radius of silicon which would lead silicon to enter the interstitial site of the ZrO_2 lattice after calcination at 450° C, and the high chloride content is probably due to Si–Cl bonding stronger than Zr–Cl, i.e. the extra chlorides are attributed to the presence of Si–Cl groups.

The transmission electron micrographs of gels and calcined powders produced from 15.35 N NH_4OH are shown in Fig. 4, and a similar appearance has been observed for other samples. There is no definite shape and size for the as-formed amorphous gels (Fig. 4a). The particles heat-treated at different temperatures show differences in morphology and appear smoother and to have more clear-cut surfaces at higher calcination temperatures (Figs 4b to f). This may be due to the surface mobility of ZrO_2 increasing with increasing calcination temperature. The crystalline size of the chloride-containing sample after calcination at 450° C lay in the range 7 to 11 nm which is consistent with the results of XRD as shown in Fig. 5. The sample calcined at 1450° C appeared to have large agglomerates (Fig. 4f).

3.2. Transformation between metastable tetragonal and monoclinic phase

Table II gives phase analysis and ratio investigations for the chloride-containing gels at different heat-treatment temperatures. Fig. 6 shows the XRD patterns of samples after calcination at 700 and 850° C. These results are consistent with infrared spectra. It is found that the sequences of transition of metastable

TABLE II Detectable phases and transition ratios in calcined Mg–PSZ by X-ray diffraction

Calcination temperature (°C)	A	B	C	D	E	F	G
No further calcination	T	T	T	T	T	T	A
700	T	T	T	T	T	T	T
750	T	T	T	T + M(?) (0.144)	T + M (0.200)	T	T
800	T + M (0.299)	T + M (0.380)	T + M (0.282)	T + M (0.263)	T + M (0.161)	T	T + M (0.317)
850	M + T (0.913)	M + T (0.915)	M + T ((0.853)	T + M (0.548)	T + M (0.288)	T	T + M (0.353)
900	M	M	M + T(?) (0.981)	M + T (0.844)	T + M (0.584)	T	M + T (0.791)
950	M	M	M	M + T (0.967)	M + T (0.925)	T + M (0.277)	M
1000	M	M	M	M	M	M + T (0.863)	M
1150	M	M	M	M	M	M	M
1250	M	M	M	M	M	M	–
1350	M	M	M	M	M	M	–
1450	M + C (0.667)	M + C (0.660)	M + C (0.610)	M + C (0.567)	M + C (0.485)	M + C(?) (0.056)	–

A = amorphous, T = metastable tetragonal, M = monoclinic, C = cubic, ? = uncertain. The numerical values in parentheses are the approximate ratios of M/M + T and C/M + C.

tetragonal to monoclinic phase are identical for both chloride-free and chloride-containing samples. The sequences of the transition for chloride-free samples and for chloride-containing samples are observed to decrease in the order A* ≈ B* > G > C* ≈ D* ≈ E* > F* and A > B > C > D > E > F, respectively.

Considering initially the chloride-free samples, the gel produced from high NH_4OH concentrations has an incompact texture with a larger pore volume and a higher surface area, as discussed previously. Therefore, compared with its surroundings, a more energetic state appears during calcination because of the extra energy supplied by the decreasing surface area, and the rate of transition will speed up when the transformation is isothermal. In addition, it is plausible that an incompact structure will undergo a smaller internal strain during calcination, which is favoured for the $T_m \rightarrow M$ transition. This argument is similar to the interpretation of Crucean and Rand [13] of the stabilization of t-ZrO_2.

The associated effects of internal strain and surface energy are reflected in the infrared spectra. In the present work, a normal Zr–O mode absorption of tetragonal Mg–PSZ is 480 cm^{-1}, 510 to 515 cm^{-1} for monoclinic phase, and 450 cm^{-1} for amorphous gels.

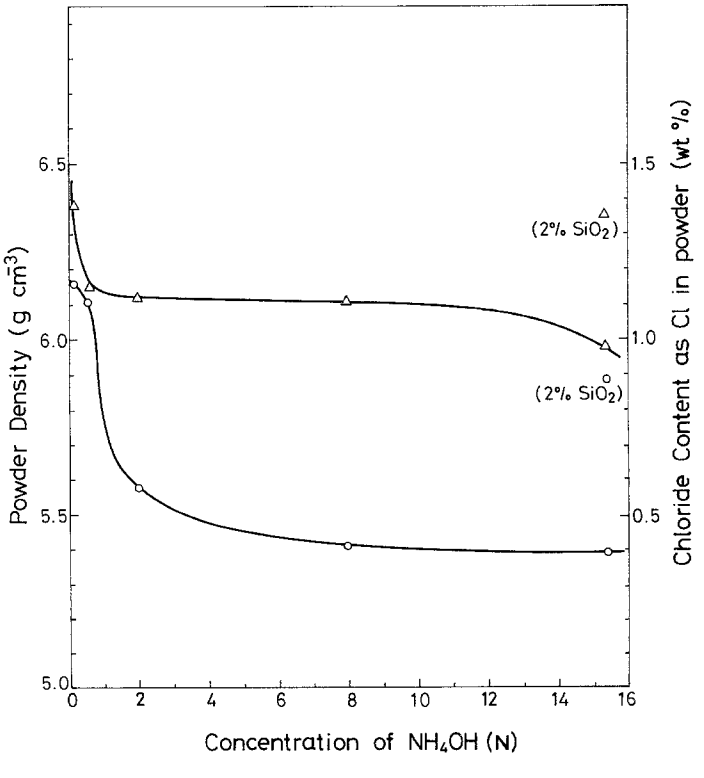

Figure 3 Relations between concentration of ammonium hydroxide, (○) powder density and (△) chloride content for chloride-containing powders.

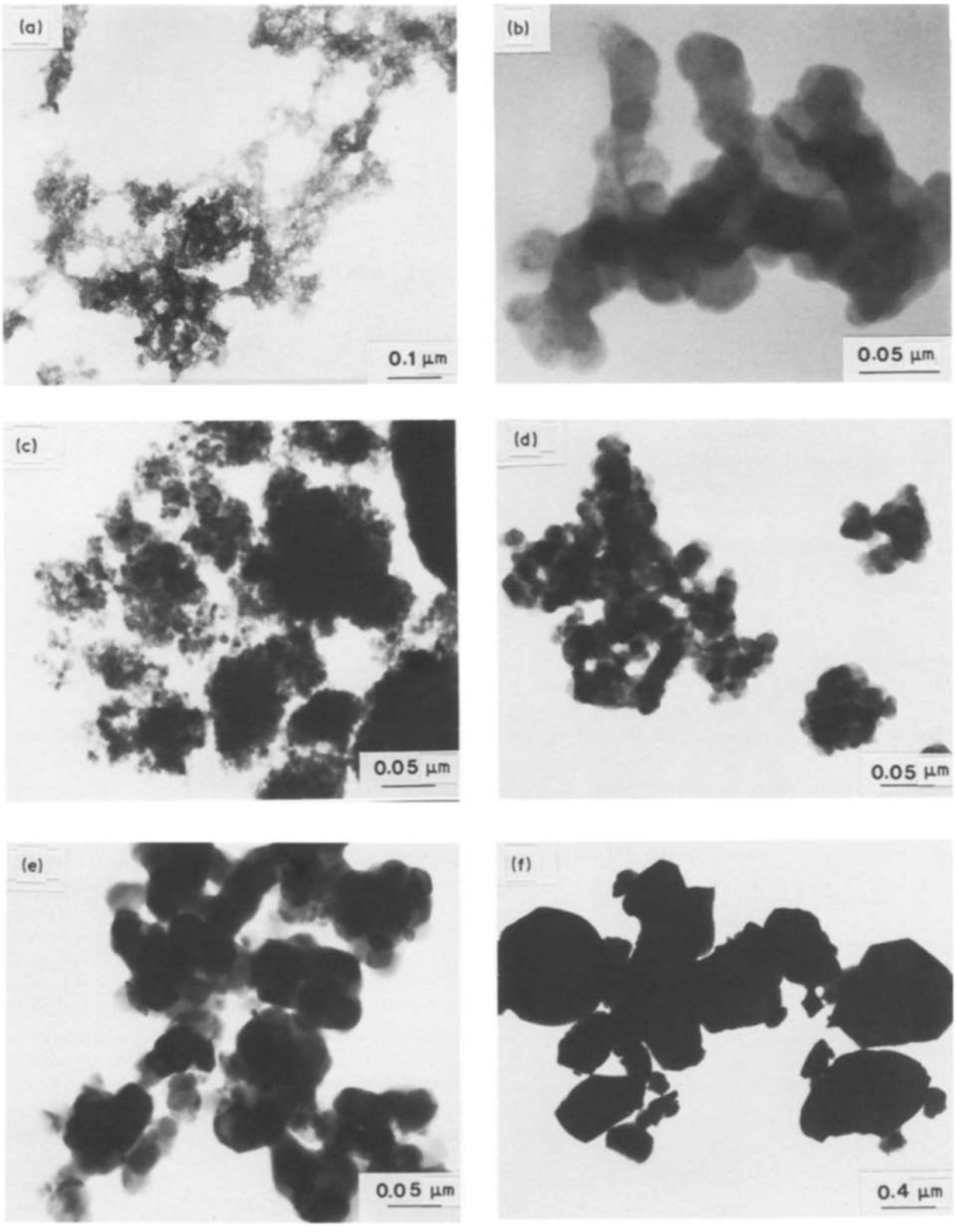

Figure 4 Transmission electron micrographs of samples (15.35 N NH_4OH). (a) As-formed gel, (b) vacuum-dried gel (sample A*), (c) 450° C, 24 h calcination (sample A), (d) 700° C, 2 h calcination (sample A), (e) 800° C, 2 h calcination (sample A), (f) 1450° C, 2 h calcination (sample A).

Previously, Livage *et al.* [9] have shown both Zr–Zr and Zr–O distances for amorphous ZrO_2 are the same as metastable tetragonal phase; however, the Zr–O distance is different for Mg–PSZ. As shown in Fig. 7, the Zr–O absorptions for the same group of samples calcined at the same temperature (700° C) shift to higher frequency with increasing NH_4OH concentration used in preparation of the samples. Similarly, the absorption for the same sample also shifts to a higher frequency when the calcination temperature is raised. Since the absorption frequency may be considered to represent the bond strength or length, it should shift to a higher frequency as the bond is compressed. It is necessary that energy must be supplied to shorten a chemical bond, and the more energetic or smaller the internal strain of the sample, the larger is the contraction of the Zr–O bond and the easier is transition. In brief, the different extents of phase transition of

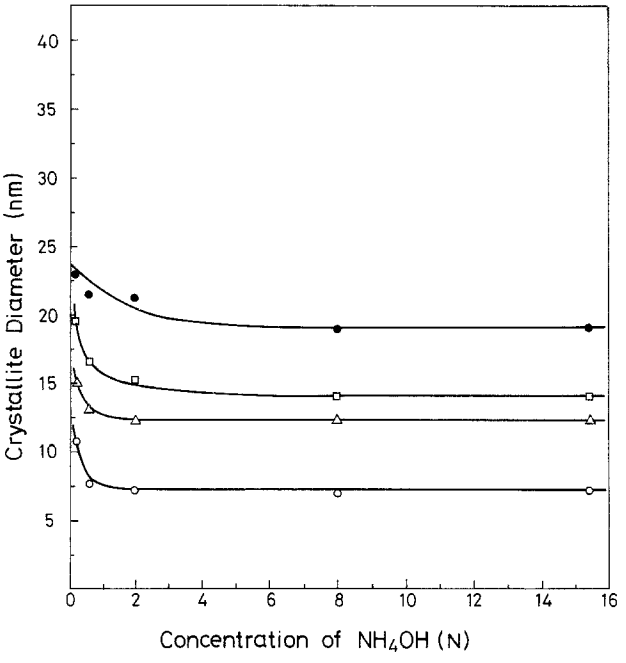

Figure 5 Effect of ammonium hydroxide concentration on crystallite size of tetragonal Mg–PSZ for chloride-containing samples. (○) 450° C, 24 h; (△) 700° C, 2 h (after 450° C, 24 h); (□) 750° C, 2 h; (●) 800° C, 2 h.

chloride-free samples may result from the differences in (1) the surface area of the gels, (2) internal strain during calcination, and (3) different compressibility of the Zr–O bond of amorphous Mg–PSZ.

The phase transition sequence of chloride-containing

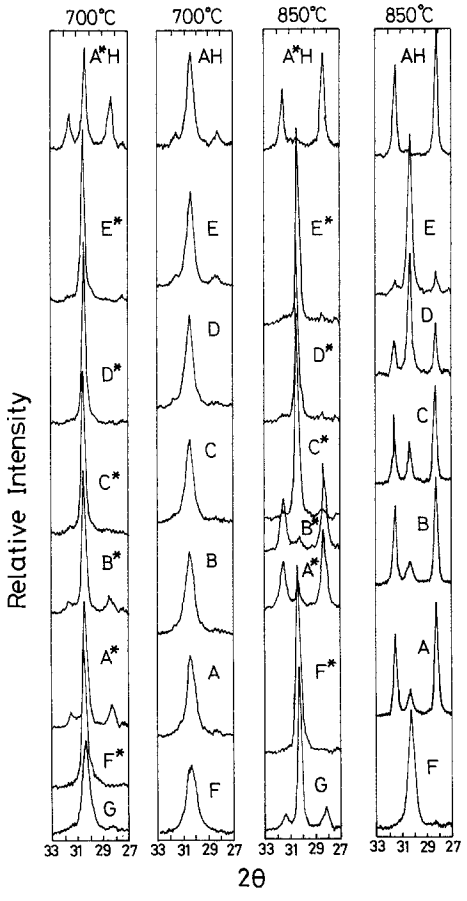

Figure 6 XRD patterns of Mg–PSZ powders calcined at selected temperatures (the reflections correspond to $(1\,1\,\bar{1})_m$, $(1\,1\,1)_t$ and $(1\,1\,1)_m$ from right to left, A*H = sample A* calcined at $H_2O(g)/N_2$, AH = sample A calcined at $H_2O(g)/N_2$).

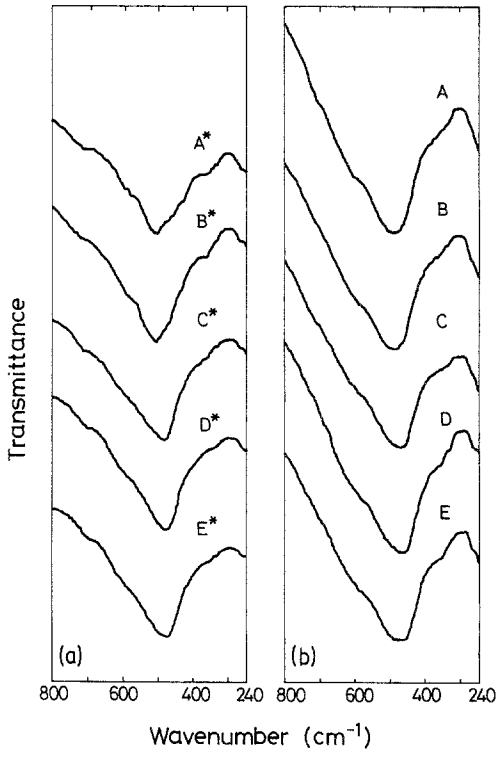

Figure 7 Infrared transmission spectra of Mg–PSZ powders calcined at 700° C, 2 h. (a) chloride-free samples, (b) chloride-containing samples.

samples, as pointed out previously, is similar to chloride-free ones. Therefore, the difference in transition has also been attributed to the same reasons, according to the facts that all Zr–O absorptions are identical for the same group starting materials (450 and 470 cm^{-1} for chloride-free and containing samples, respectively), and similar infrared and XRD results were obtained. A feature in this group is that the crystallite size of the tetragonal phase (starting materials) increases with decreasing concentration of NH_4OH (as shown in Fig. 5), and which should result from the difference in the texture of gel, i.e. the denser the gel the larger the crystallite size. The effects of crystallite size on transformation has been pointed out by Garvie [23], and is consistent with the sequence of $T_m \rightarrow M$ transformation in the present work. One major difference in phase transition between chloride-free and chloride-containing samples is that the transition temperature or rate of the latter is lower than the former, for samples derived from 2 N, 0.6 N, and 0.2 N NH_4OH (C–C*, D–D*, E–E*), but the reverse for the others (G, A–A*, B–B*). A probable explanation is given by Osendi *et al.* [12], i.e. $T_m \rightarrow M$ transition takes place by the elimination of defects which arise from the evolution of volatile impurities, and larger amounts of impurities are favoured for transition. Therefore, explanations for the present case are probably: (1) the total amount of impurities for samples C, D, and E (sum of Cl and OH groups) is more than that of C*, D* and E* (OH group only), but the inverse for samples A, B, and G; (2) the presence of chlorine has lowered the critical crystallite size because the HCl evolved to the gas phase is easier than H_2O. Garvie [8] has shown that the surface energy of monoclinic ZrO_2 is greater than that of the

tetragonal phase, so that the decreasing critical crystallite size of the $T_m \rightarrow M$ transition is to be expected. Indeed, decreasing critical crystallite size of the $T_m \rightarrow M$ transition has been observed in the present work, and the difference is about 10 to 15 nm.

The influences of water vapour and silica on the $T_m \rightarrow M$ phase transition have been observed and are shown in Fig. 6. As observed by Murase and Kato [24] in the phase transformation of ZrO_2, water vapour also promotes the $T_m \rightarrow M$ transition of Mg–PSZ (see A–AH and A*–A*H in Fig. 6). In fact, transition temperatures of A and A* under an $H_2O(g)/N_2$ atmosphere have been observed at 600 and 700° C, respectively, and a reduction on the critical crystallite size has been found. On the other hand, the transition temperatures of silica-containing samples F and F* are 150 and 200° C higher than those of A and A*, respectively. An inhibition of the normal $T_m \rightarrow M$ transition had been suggested by Clark and Reynolds [7] because a keying action was exerted by silica on ZrO_2. For the present work, the keying action has been considered to stem from the induction of strains by silica which is located at interstitial sites of the ZrO_2 lattice and therefore stabilized the tetragonal Mg–PSZ. In addition, it is found that both growth of tetragonal and monoclinic crystals can be inhibited by the presence of silica.

3.3. Formation of cubic phase

The XRD patterns and infrared spectra after 2 h calcination at 1450° C are shown in Figs 8 and 9. The cubic phase appears up to 1450° C for both chloride-free and chloride-containing samples. The phases present at 1450° C should be tetragonal and cubic phases in coexistence taking into account the phase diagram [16, 25]. However, only a mixture of monoclinic and cubic phase was obtained in present case. Heuer [26] and Porter and Heuer [27] have shown that c-ZrO_2 (ss) decomposed into c-ZrO_2 (ss) and t-ZrO_2 (ss) after ageing at 1400 to 1500° C, and t-ZrO_2 will transform to the monoclinic phase spontaneously if the size of the tetragonal plate exceeds a critical value (0.2 μm for Mg–PSZ [26]). Thus the formation of a mixture of cubic and monoclinic phases after quenching from 1450° C is reasonable in the present work.

The rate of formation of cubic phase at 1450° C is found to be in the following sequences: $E^* \approx D^* \approx C^* > B^* \approx A^* > F^*$ and $A > B > C > D > E > F$. Sample F* has not transformed to cubic phase and sample F has an uncertain ($\sim 5\%$) amount of transformation. To explain this significant difference in phase transformation between the two groups of samples, two transformation paths are proposed: $A \rightarrow [T_m] \rightarrow [M] \rightarrow [T] \rightarrow T + C$ for chloride-free samples and $T_m \rightarrow T \rightarrow T + C$ for chloride-containing samples, where A, T, T_m, M and C denote amorphous, high-temperature tetragonal phase, metastable tetragonal phase, monoclinic phase, and cubic phase, respectively. The bracket indicates an intermediate state which forms and disappears rapidly. For chloride-free samples, it is possible that samples derived from higher NH_4OH concentrations

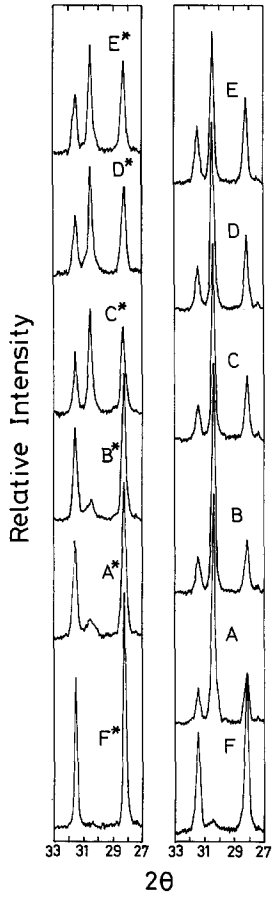

Figure 8 XRD patterns of Mg–PSZ powders calcined at 1450° C, 2 h. (The reflections are $(1\,1\,\bar{1})_m$, $(1\,1\,1)_c$ and $(1\,1\,1)_m$ from right to left).

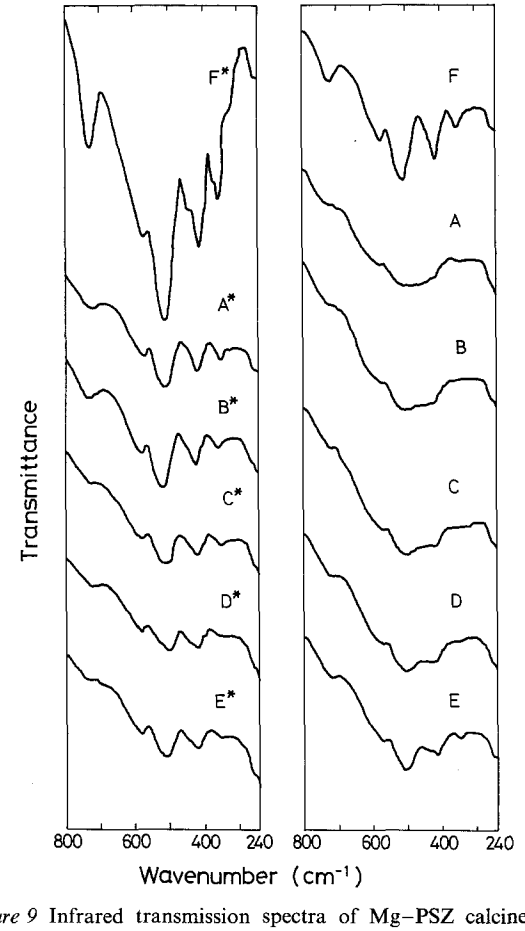

Figure 9 Infrared transmission spectra of Mg–PSZ calcined at 1450° C, 2 h.

will transform easily into the monoclinic phase (with a smaller internal strain during calcination), therefore the rate of formation of high-temperature tetragonal phase is slower and thus leads to a smaller amount of tetragonal and cubic phase by considering the equilibrium between the cubic and tetragonal phase. Therefore the [M] → [T] transition is the rate determining step for the formation of the cubic phase. On the other hand, the initial chloride-containing materials are metastable tetragonal phase, so that only a negligible amount follows the $T_m \rightarrow [M] \rightarrow T$ path and the main parts follow the $T_m \rightarrow T$ path by considering the structural similarity. In other words, samples derived from higher NH_4OH concentrations will convert easily to the cubic phase because of a smaller internal strain in the starting materials.

As shown in Fig. 8, it has been found that the amount of cubic phase in chloride-containing samples is more than in chloride-free samples, i.e. the former has a faster transition rate. This difference may be attributed to (1) omission of intermediate steps, and (2) HCl evolved to the gas phase is faster than H_2O which probably favours transition.

As in its influence on the $T_m \rightarrow M$ transition, silica also inhibits the tetragonal-to-cubic transformation. The inhibitive ability has been attributed to the formation of magnesium silicates which are thermodynamically more stable at high temperatures and thus lower the effective content of MgO on raising the transition temperature.

4. Conclusions

1. The properties and structures of ZrO_2–8.1 mol % MgO gels are strongly affected by the preparation conditions. A gel produced from dilute NH_4OH solution has a smaller pore volume and pore size, which results in a denser, high chloride and rigid calcined powder.

2. The samples derived from higher NH_4OH concentrations have a lower crystallization temperature and faster rate of $T_m \rightarrow M$ transformation. The difference in transformation has been attributed to the difference in surface energy and internal strain during calcination, which leads to the difference in compressibility of the Zr–O bond of the amorphous and starting metastable tetragonal materials.

3. For chloride-containing samples, the rate of tetragonal-to-cubic transformation at 1450° C is increased with increasing NH_4OH concentration used in the preparation of samples, but the inverse sequence is true for chloride-free samples. The difference in phase transformation between both groups is attributed to the probable different transition paths. The difference in transformation within the same groups has been interpreted by considering the effect of internal strain which is favoured for stabilization of the tetragonal phase.

4. The $T_m \rightarrow M$ transition of Mg–PSZ was promoted by water vapour and chlorides, but inhibited by SiO_2. In addition, the T → C transition is also inhibited by SiO_2.

Acknowledgements

The authors thank Miss L. E. Chiang, the Chemical Industry Institute of the Industrial Technology Research Institute, ROC, for her help with X-ray diffraction.

References

1. G. M. WOLTEN, *J. Amer. Ceram. Soc.* **46** (1963) 418.
2. E. C. SUBBARAO, H. S. MAITI and K. K. SRIVASTAVA, *Phys. Status Solidi A* **21** (1974) 9.
3. D. K. SMITH and C. F. CLINE, *J. Amer. Ceram. Soc.* **45** (1962) 249.
4. H. NISHIZAWA, N. YAMASAKI and K. MATSUOKA, *ibid.* **65** (1982) 343.
5. K. S. MAZDIYASNI, C. T. LYNCH and J. S. SMITH, *ibid.* **49** (1966) 286.
6. I. A. EL-HANSHOURY, V. A. RUDENKO and I. A. IBRAHIM, *ibid.* **53** (1970) 264.
7. G. L. CLARK and D. H. REYNOLDS, *Ind. Eng. Chem.* **29** (1937) 711.
8. R. C. GARVIE, *J. Phys. Chem.* **69** (1965) 1238.
9. J. LIVAGE, K. DOI and C. MAZIERES, *J. Amer. Ceram. Soc.* **51** (1968) 349.
10. T. MITSUHASHI, M. ICHIHARA and U. TATSUKE, *ibid.* **57** (1974) 97.
11. E. TANI, M. YOSHIMURA and S. SOMIYA, *ibid.* **66** (1983) 11.
12. M. I. OSENDI, J. S. MOYA, C. J. SERNA and J. SORIA, *ibid.* **68** (1985) 135.
13. E. CRUCEAN and B. RAND, *Trans. J. Brit. Ceram. Soc.* **78** (1979) 58.
14. B. E. YOLDAS, *J. Amer. Ceram. Soc.* **65** (1982) 387.
15. *Idem*, in "Ultrastructure Processing of Ceramics, Glasses, and Composites", edited by L. L. Hench and D. R. Ulrich (Wiley, New York, 1984) p. 60.
16. D. VIECHNICKI and V. S. STUBICAN, *J. Amer. Ceram. Soc.* **48** (1965) 292.
17. M. D. SACKS and T. Y. TSENG, *ibid.* **67** (1984) 526.
18. American Public Health Association etc. (ed.) "Standard Method for Examination of Water and Waste Water" (American Public Health Association, Washington, D.C., 1981) p. 269.
19. H. P. KLUG and L. E. ALEXANDER, "X-Ray Diffraction Procedures" (Wiley, New York, 1954) Ch. 9.
20. R. C. GARVIE and P. S. NICHOLSON, *J. Amer. Ceram. Soc.* **55** (1972) 303.
21. P. A. EVANS, R. STEVENS and J. G. P. BINNER, *Trans. J. Brit. Ceram. Soc.* **83** (1984) 39.
22. W. B. BLUMENTHAL, "The Chemical Behavior of Zirconium" (Van Nostrand, Princeton, 1958) p. 181.
23. R. C. GARVIE, *J. Phys. Chem.* **82** (1978) 218.
24. Y. MURASE and E. KATO, *J. Amer. Ceram. Soc.* **66** (1983) 196.
25. C. F. GRAIN, *ibid.* **50** (1967) 288.
26. A. H. HEUER, in "Science and Technology of Zirconia", edited by A. H. Heuer and L. W. Hobbs (The American Ceramic Society, Columbus, Ohio, 1981) p. 98.
27. D. L. PORTER and A. H. HEUER, *J. Amer. Ceram. Soc.* **62** (1979) 298.

Received 8 July
and accepted 21 July 1986